

PACS numbers: 78.67.Bf; 87.16.dp; 42.30.Wb; 87.63.lm; 87.57.cj
DOI: 10.1070/QE2012v042n06ABEH014884

Visualisation of distribution of gold nanoparticles in liver tissues *ex vivo* and *in vitro* using the method of optical coherence tomography

E.A. Genina, G.S. Terentyuk, B.N. Khlebtsov, A.N. Bashkatov, V.V. Tuchin

Abstract. **The possibility of visualising the distribution of gold nanoparticles in liver by means of the method of optical coherence tomography is studied experimentally in model samples of beef liver *in vitro* and rat liver *ex vivo*. In the experiments we used the gold nanoparticles in the form of nanocages with resonance absorption in the near-IR spectral region. In the model studies the suspension of nanoparticles was applied to the surface of the sample, which then was treated with ultrasound. In the *ex vivo* studies the suspension of nanoparticles was injected to the laboratory rats intravenously. The image contrast and the optical depth of detection of blood vessels and liver structure components are calculated, as well as the depth of liver optical probing before and after the injection of nanoparticles. It was shown that the administration of the nanoparticle increases significantly the imaging contrast of liver blood vessels owing to the localisation of the nanoparticles therein.**

Keywords: *optical coherence tomography, gold nanoparticles, nanocages, image contrast, liver.*

1. Introduction

The use of nanomaterials as contrasting agents for cell visualisation [1, 2], carriers for delivering drugs and photosensitizers to the target cells [3, 4], agents that allow implementation of hyperthermia of labelled cells without heating the adjacent healthy tissue [5, 6] and other applications is a new trend in modern medicine. Metal nanoparticles with plasmon resonance are of particular interest for biomedicine because of their unique optical and physicochemical properties, since it is well known that the resonance absorption of light by a metal nanoparticle may be tuned into the desired optical range by varying their size, shape, material, and structure [6–9]. Moreover, the use of gold nanoparticles as patterns and nanocontainers allows obtaining multifunction nanostructures for theranostics (therapy and diagnostics) on their base [10–12].

In modern medicine an urgent problem is how to provide efficient delivery of growth factors and other drugs to the liver in order to promote regeneration of this organ [13–15]. The use of gold nanoparticles for this goal seems well grounded. On the one hand, it is well known that, thanks to the branched vascular network present in the liver, the nanoparticles accumulate in this organ after their peroral, intraperitoneal, or intravenous administration [13–15]. The conjugation of drugs with nanoparticles allows essential enhancement of their accumulation and reduce the toxicity [6, 7]. On the other hand, the resonance absorption of light by gold nanoparticles allows their visualisation in organs and tissues by means of optical (noninvasive) methods [7, 8], which make it possible to monitor the accumulation of nanoparticles in the liver and to measure the pharmacokinetic parameters of the process.

The properties of plasmon nanoparticles may be efficiently used also in laser thermotherapy of tumour neoplasms in liver. Usually, in the course of the interstitial laser thermotherapy the optical fibre is introduced directly into the tissue of the tumour; the irradiation is performed in the near IR range [16, 17]. In this case the main problem is the thermal damage of healthy cells, surrounding the tumour. However, in the case of using the laser radiation with the wavelength, corresponding to the plasmon resonance in nanoparticles, it becomes possible to perform the local heating of nanoparticles and, therefore, to provide destruction of labelled cells without heating of the adjacent biotissue [5, 18].

Monitoring of accumulation of gold nanoparticles in liver plays an important role in all mentioned applications. Real-time visualisation of nanoparticles inside the organ allows better evaluation of their pharmacokinetics and determination of localisation in the biotissue.

Among the variety of optical methods of visualising gold nanoparticles in biotissues, the method of optical coherence tomography (OCT) is of particular importance [19, 20]. OCT is a noninvasive method of visualising the internal structure of optically inhomogeneous objects, based on the principles of low-coherency interferometry, in which the light of the near-IR range (0.75–1.3 μm) is used [21–23]. The method allows investigation of the internal microstructure of biotis-

E.A. Genina, A.N. Bashkatov N.G. Chernyshevsky Saratov State University (National Research University), Research-Educational Institute of Optics and Biophotonics, ul. Astrakhanskaya 83, 410012 Saratov, Russia;
G.S. Terentyuk N.G. Chernyshevsky Saratov State University (National Research University), ul. Astrakhanskaya 83, 410012 Saratov, Russia; Ulyanovsk State University, ul. Tolstogo 42, 432000 Ulyanovsk, Russia; V.I. Razumosky Saratov State Medical University, ul. Bol'shaya Kazach'ya 112, 410012 Saratov, Russia; e-mail: vetklinika@front.ru;
B.N. Khlebtsov Institute of Biochemistry and Physiology of Plants and Microorganisms, Russian Academy of Science, prosp. Entuziastov 13, 410049 Saratov, Russia; e-mail: bkhl@ibppm.sgu.ru;
V.V. Tuchin N.G. Chernyshevsky Saratov State University (National Research University), ul. Astrakhanskaya 83, 410012 Saratov, Russia; Institute for Problems of Precise Mechanics and Control, Russian Academy of Sciences, Rabochaya ul. 24, 410028 Saratov, Russia; University of Oulu, P.O. Box 4500, FIN-90014, Oulu, Finland; e-mail: tuchinvv@mail.ru

Received 23 April 2012.
Kvantovaya Elektronika **42** (6) 478–483 (2012)
Translated by V.L. Derbov

sues at the depth up to 2 mm with the spatial resolution 10–15 μm without breaking their integrity [21–24]. In a number of papers [19, 20, 25] it is shown that the gold nanoparticles, introduced into a biological tissue, enhance the contrast of the OCT image of this biotissue. In [26] it was also noticed, that the presence of metal nanoparticles in blood vessels of liver leads to the enhancement of the OCT signal from them, which offers an opportunity to visualise them.

The aim of the present paper is to investigate the possibility of visualisation of gold nanocages distribution in liver tissues by means of the OCT method both in model experiments *in vitro* and under the preliminary *in vivo* intravenous injection of nanoparticles.

2. Materials and methods

Gold nanoparticles used in the experiments were obtained by means of the two-stage process, described in detail earlier [27]. At the first stage in the course of polyol synthesis reaction induced by sodium sulphide the silver nanocubes were obtained with the mean size of ~45 nm, which then played the role of a template in the reaction of galvanic substitution. As a result hollow and porous gold nanoparticles were obtained with the size ~50 nm (in the literature they are referred as nanocages) [25, 28].

Figure 1 presents images of the used nanoparticles, obtained by the aid of the Libra 120 electron microscope (Carl Zeiss, Germany, magnification 40000$^{\times}$), and the optical density spectrum of the aqueous suspension of nanoparticles with the concentration of gold in the suspension ~100 μg mL^{-1}, measured using the Specord 250 spectrophotometer (Analytik Jena, Germany). It is seen that the nanoparticles preferably possess the shape of a cube with the size of about 50 μm. The colloid demonstrates resonance absorption in the region of biotissue transparency window at the wavelength 785 nm.

For the experiments we used the suspension of nanoparticles in saline (0.9% aqueous solution of NaCl). The surface of nanocages was preliminarily coated with a layer of polyethylene glycol with molecular weight 400 (PEG400). The concentration of nanoparticles in the suspension was 100 μg mL^{-1} and the optical density was 19. This value of the optical density was obtained by approximating the optical density of the colloid diluted by 20 times, measured in the cuvette 1 cm thick.

For the series of model experiments we used beef liver *in vitro*. Twenty samples were cut having the size of about 3×3×1 cm. The samples were not frozen. Ten samples were left intact and in ten samples the fibrous tunic was removed. The samples were placed in Petri dishes and moistened with saline to prevent drying in the process of investigation. The experiments were performed at the room temperature (~20 °C).

The model samples were divided into three groups: (i) control samples; (ii) experimental samples, to the surface of which a thin layer of suspension of nanoparticles was applied (exposure 30 min), and then the nanoparticles were removed from the surface of the sample; (iii) experimental samples, to the surface of which the suspension of nanoparticles was applied and then the ultrasound (US) treatment of the surface was performed.

The US treatment was used to increase the penetration depth of nanoparticles and to make their distribution within the liver tissues more uniform. As a source of ultrasound we used the Dinatron 125 ultrasound transducer (Dinatronics,

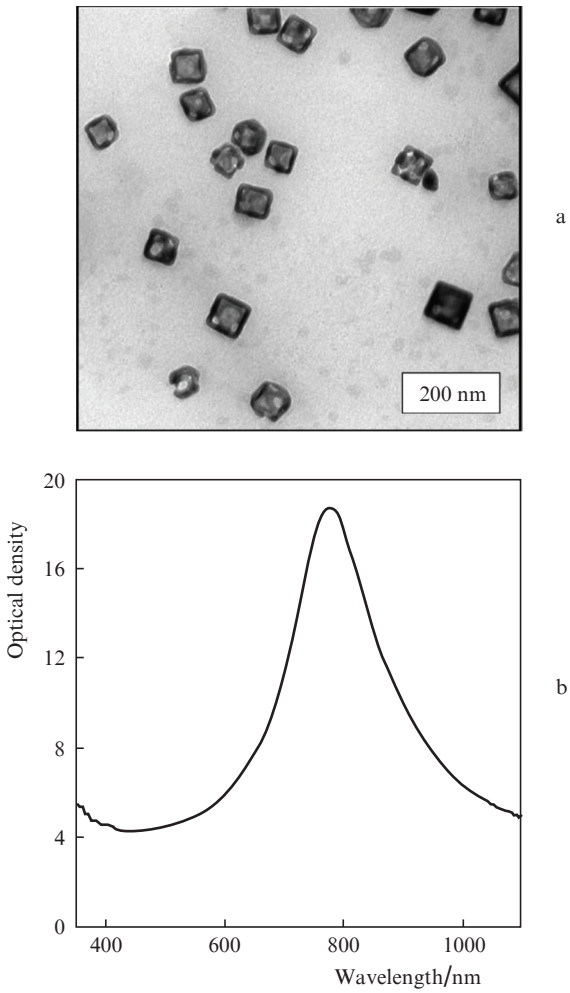

Figure 1. Images of gold nanocages, obtained using electron microscopy (a) and optical density spectrum of aqueous suspension of nanocages (b). The concentration of gold in the suspension is ~100 μg mL^{-1}.

USA). The US frequency was 1 MHz, the power density was 1.5 W cm^{-2} in the continuous-wave regime, and the time of US exposure was 10 min.

For the series of *ex vivo* experiments the liver was extracted from four white outbred rats. The weight of each animal was about 200 g. The injection of the preparation was done into the hip vein; the volume of injected suspension was 2 mL kg^{-1}. After 24 hours the liver was extracted from the abdominal cavity, but was not cut. From one half of the whole sample the fibrous tunic was removed, while the second one was left intact.

The samples were divided into two groups: (i) the control samples, obtained from the animals not subjected to any treatment; (ii) the experimental samples, obtained from the animals, to which the suspension of nanoparticles was injected intravenously. Each group included two intact regions from two samples and two regions with remover fibrous tunic also from two samples.

The monitoring of nanoparticles in the liver tissues was implemented by means of the optical Thorlabs Spectral Radar OCT coherence tomograph (OCP930, Thorlabs, USA) at the wavelength 930 nm. The OCT scanning was performed before and after the appropriate treatment (depending on the group) of the samples of beef liver in the *in vitro* studies and directly after extracting the liver from the rat in the *ex vivo* studies.

The contrast C of the image of the liver blood vessels in the OCT images was evaluated using the formula

$$C = \frac{R_1 - R_2}{R_1 + R_2}, \quad (1)$$

where R_1 and R_2 are the maximal and the minimal amplitude of the OCT signal, averaged over 3–5 A-scans in the region of inhomogeneity (Fig. 2). In the model experiments *in vitro* the values of the contrast were calculated at the depths 300 and 500 μm, while in the experiments *ex vivo* it was determined at the optical depth ~200 μm. The contrast was calculated in the longitudinal and the transverse direction in the region of inhomogeneity, observed in the OCT images. The results were averaged, and the root-mean-square deviation (sd) was calculated.

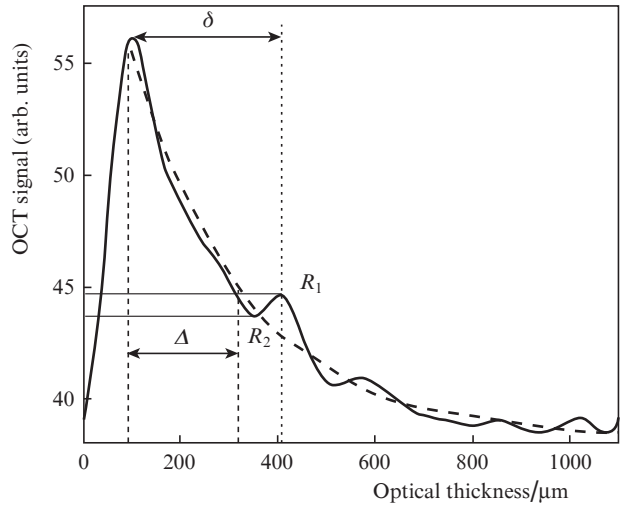

Figure 2. Averaged A-scan of the liver OCT image (R_1 and R_2 are the maximal and the minimal amplitudes of the OCT signal at the boundaries of the inhomogeneity, respectively; Δ is the optical depth of probing; δ is the optical depth of detection).

The optical depth of probing Δ was estimated as the depth, at which the OCT signal is weakened by e times; the obtained results were averaged over five A-scans in three regions of the image and the value of sd was calculated. The optical depth δ of object detection inside the tissue was determined as the distance between the intensity maxima of the signals from the sample surface and the most deeply located object, which could be seen in the image (Fig. 2).

3. Results and discussion

As known, the structure of liver is rather nonuniform. By its structure the liver is a complex branched tubular gland, penetrated by blood vessels and bile ducts. The basic morphologic and functional unit of liver is a hepatocyte. Hepatocytes form lobules of liver, each having the shape of a prism. In the centre of each lobule a central vein is located. Between the lobules there is a small amount of connective tissue, in which blood vessels and bile ducts are located. The volume of a lobule is penetrated by sinusoidal capillaries [29]. Hepatocytes make about 60% of the liver mass [30]. From the outside the liver is coated by serous tunic, under which there is a thin and dense fibrous tunic. The latter penetrates into the liver depth and surrounds the blood vessels [29].

Figure 3 presents the results of OCT scanning of the intact liver samples, namely, the control sample, as well as the samples treated with the suspension of nanoparticles without ultrasound and with it. On the surface of all presented samples the fibrous tunic is well-seen (shown by the short arrow), and in the samples, treated with the suspension of nanoparticles, blood vessels are visualised.

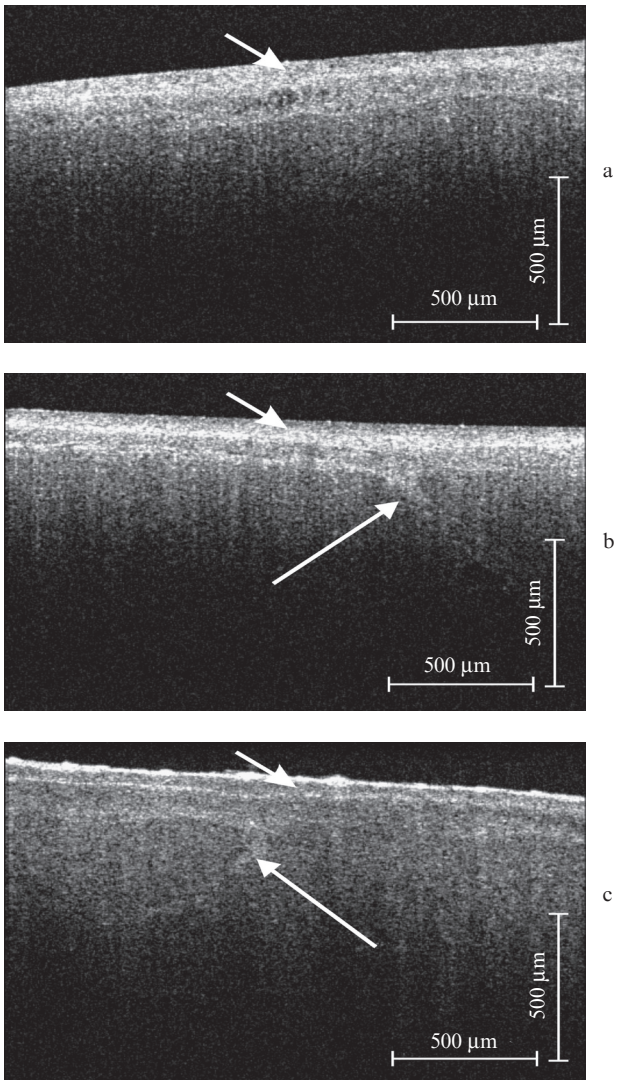

Figure 3. OCT images of the intact liver samples: the control sample (a); the sample, exposed to the suspension of nanoparticles during 30 min (b); the sample with the suspension of nanoparticles, applied to the surface, treated with ultrasound during 10 min (c).

The indistinguishability of the blood vessel network in the OCT image of the intact liver sample (Fig. 3a) is due to the fact that the mean refractive indices of the liver tissue (1.38 [31]) and the walls of the blood vessels penetrating the liver (1.36–1.39 [31]) at the OCT scanning wavelength practically coincide. Although in the case of *in vivo* experiments the blood vessels in the OCT images are seen relatively well [32], which is due to higher refractive index of blood (1.4 [31]), in the case of *in vitro* measurements the vessels, especially at the surface of the sample, are hollow, due to which their images

remain non-contrast. It follows from the analysis of Fig. 3a that the optical probing depth in the intact liver is 353 ± 59 μm.

In Figs 3b and c it is clearly seen that the nanoparticles are distributed along the boundaries of the tunic and penetrate into the blood vessel (pointed by the long arrow), which is seen by the OCT signal increase. Since the specific absorption and scattering of light in the IR spectral range for nanoparticles is hundreds of times greater than those of the surrounding biotissues [25], the reflection of light from the boundary between the biotissue and the particle makes it possible to observe the images of objects, in which nanoparticles are located, in particular, blood vessels. The mean values of the contrast of blood vessels image in these samples are similar; however, the depth of their detection differs by nearly two times. At the same time, from Fig. 3b it is seen that surface application of nanoparticles leads to essential decrease (to 235 ± 29 μm) of the optical depth of liver tissue probing, which is due to the screening effect produced by the nanoparticles applied to the biotissue surface because of their high reflectivity that hampers the penetration of the probing radiation into the biotissue. The estimates of the contrast values and the optical depth of probing and detection for all samples are summarised in Table 1.

As seen from Fig. 3c, the US treatment results in a more uniform distribution of nanoparticles in the tissues of the liver and promotes their penetration into the tissue depth via the blood vessels. In this case the concentration of nanoparticles in the tunic is reduced, which is seen by the reduction of the image contrast the increase in the mean optical depth of biotissue probing up to 412 ± 59 μm, and the mean optical depth of blood vessels detection up to 617 ± 54 μm (see Table 1).

Figure 4 presents the results of OCT scanning of liver samples with removed fibrous tunic, the control sample and the samples treated with suspension of nanoparticles without ultrasound and with it. The mean values of the depth of probing of the intact sample (353 ± 59 μm, Fig. 3a) and the one with removed fibrous tunic (357 ± 46 μm, Fig. 4a) are nearly equal. The detected objects in this case were located in the region of probing. However, in the absence of fibrous tunic the depth of detection of blood vessels in the liver after the introduction of nanoparticles increased in comparison with intact samples (see Table 1) by almost two times, from 358 ± 21 to 630 ± 93 μm. Thus in the images of some samples the blood vessels and lobules of the liver were visualised at the depth greater than 700 μm (see Figs 4b and c, labelled with letters). The use of ultrasound facilitated the increase in the image contrast of deeply located liver blood vessels in comparison with both intact samples and the ones not treated with ultrasound (see Table 1); in this case the number and detailing of the observed structure elements (Fig. 4c) in the OCT images also increased. This is explained by the fact that the fibrous tunic serves as a certain filter for nanoparticles, introduced into deeper layers of the liver tissue, and the number of particles, penetrating into blood vessels, in insufficient for producing their high-contrast image.

Figures 5a, b present the OCT images of control samples of rat liver *ex vivo*, the intact one and the one with removed fibrous tunic, and in Figs 5c, d we can see the OCT images of the rat liver samples in 24 hours after intravenous *in vivo* injection of the suspension of nanoparticles in the cases of non-removed and removed fibrous tunic. In the image of the intact liver sample *ex vivo* (Fig. 5a), in contrast to the images of the *in vitro* samples (Fig. 3a), the structure of the fibrous

Table 1. Contrast of imaging the inhomogeneities in A-scans of the OCT liver images and optical depths of probing the samples and of detection of contrast objects in the volume of the samples.

Series	Description of samples		Number of samples	Mean value and root-mean-square deviation (±sd) of the image contrast at different optical depths	Mean value and root-mean-square deviation (±sd) of the optical depths of probing/μm	Mean value and root-mean-square deviation (±sd) of the optical depths of detection/μm
In vitro*	Control	Intact	2	0/0	353 ± 59	205 ± 66
		Fibrous tunic removed	2	0.03 ± 0.01/0	357 ± 46	265±47
	Topical administration of nanoparticle suspension	Intact	4	0.07 ± 0.02/0	235 ± 29	358 ± 21
		Fibrous tunic removed	4	0.05 ± 0.02/0.07 ± 0.02	353 ± 46	630 ± 93
	Topical administration of nanoparticle suspension and US treatment	Intact	4	0.07 ± 0.04/0.02 ± 0.01	412 ± 59	617 ± 54
		Fibrous tunic removed	4	0.15 ± 0.04/0.1 ± 0.04	353 ± 46	679 ± 73
Ex vivo**	Control	Intact	2	0.07 ± 0.02	431 ± 59	147 ± 59
		Fibrous tunic removed	2	0	235 ± 93	–
	Intravenous injection of the suspension of nanoparticles	Intact	2	0	462 ± 94	–
		Fibrous tunic removed	2	0.11 ± 0.02	353 ± 53	235 ± 23

*The contrast is calculated for the optical depths 300 and 500 μm; **the contrast is calculated for the optical depth 200 μm.

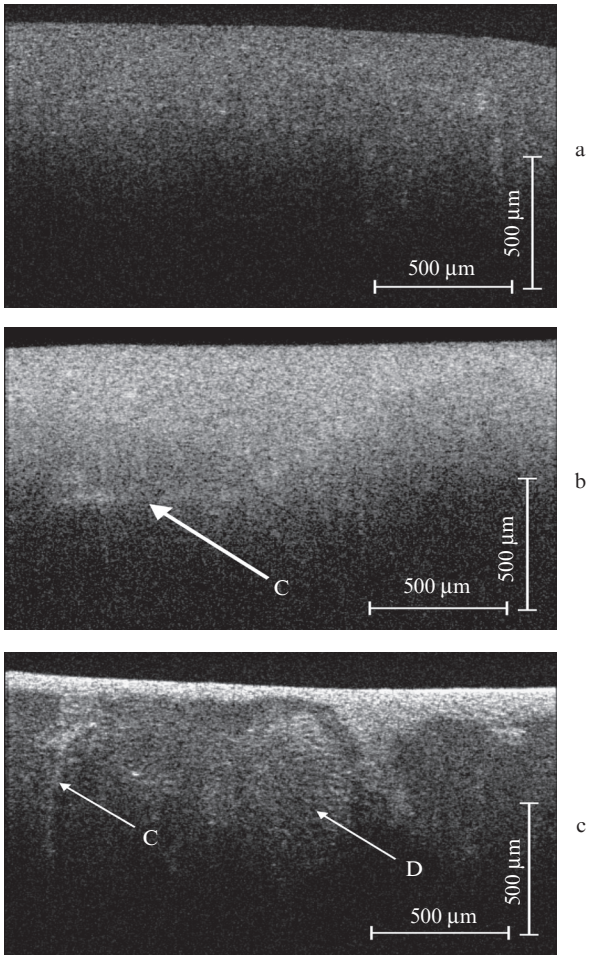

Figure 4. OCT images of the liver samples with removed fibrous tunic: the control sample (a); the sample, exposed to the suspension of nanoparticles during 30 min (b); the sample with the suspension of nanoparticles, applied to the surface, treated with ultrasound during 10 min (c) (C – blood vessel, D – liver lobule).

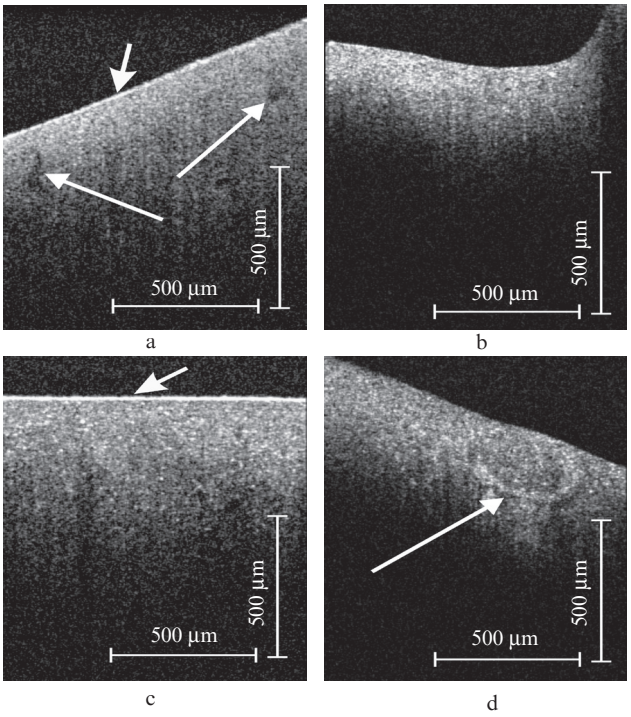

Figure 5. OCT images of the samples of rat liver *ex vivo*: the control (intact) sample (a); the control sample with removed fibrous tunic (b); the sample in 24 hours after intravenous *in vivo* injection of suspension of nanoparticles without removal of fibrous tunic (c); the sample of the rat liver sample in 24 hours after intravenous *in vivo* injection of the suspension of nanoparticles with removed fibrous tunic (d).

tunic (marked with the short arrow) is not visualised. Possibly, it is due to both the difference in the liver structure (the fibrous tunic of the rat liver is much thinner than that of the beef liver) and the time of keeping the samples in air before the beginning of experiments (at longer keeping the samples in open air the tunic could become denser because of dehydration, which enhances the contrast of imaging). However, in Fig. 5a the inhomogeneities in the form of shaded regions are well seen (marked with long arrows), which may correspond to the cross sections of blood vessels, filled with blood. Nevertheless, the contrast of the image of these inhomogeneities is essentially lower than the contrast of the image of a vessel containing nanoparticles (see Table 1), which is due to significant reflectance of nanoparticles. In Fig. 5d the blood vessel (marked with an arrow) is visualised rather distinctly, with a high degree of contrast.

In Figs 5b and c no significant inhomogeneities are visualised, and integrally in the images of the samples (control, with removed fibrous tunic, experimental intact) it appeared impossible to determine the contrast values.

From the analysis of the obtained results it is possible to conclude that gold nanoparticles are efficiently accumulated in liver tissues and enhance the contrast of the blood vessels image, which allows visualisation of their distribution in the biotissue.

4. Conclusions

Thus, the model experiments on introducing nanocages into the liver tissues have shown that, when the suspension of nanoparticles is applied to the surface of intact samples, the nanoparticles mainly spread along the surface of the liver fibrous tunic and penetrate into larger blood vessels. Under the action of ultrasound the high-contrast visualisation and object detection may be performed at the optical depth up to 700 μm at the wavelength of the probing radiation 930 nm. In the absence of fibrous tunic we managed to increase the contrast by more than two times at the depth of 300 μm and by five times at the depth 500 μm, as compared with the intact samples, and to attain a 10% increase in the biotissue probing depth.

As a result of the OCT investigation of the *ex vivo* liver tissue in 24 hours after intravenous injection of the suspension of nanoparticles we obtained high-contrast images of liver blood vessels at the depth ~200 μm due to localisation of gold nanoparticles in them. The contrast of blood vessel images was increased by more than 1.5 times.

The results of the present study may be used for controlling the delivery of nanoparticles into the liver aimed at hyperthermia of neoplasms or therapy of such liver diseases as cirrhosis, hepatitis, etc.

Acknowledgements. The work was carried out in the framework of State Contract No. 02.740.11.0879 and was sup-

ported by the Grant of the RF President (Grant No. NSh-1177.2012.2 for Support of Scientific Schools), by the Ministry of Education and Science of Russia (Research Grant No. 0121158566), by the European Commission (7th Frame Programme – Photonics4Life, Grant No. 224014), and by the Program FiDiPro TEKES (40111/11), Finland.

References

1. Schrand A.M., Braydich-Stolle L.K., Schlager J.J., Dai L., Hussain S.M. *Nanotechnology*, **19**, 235104 (2008).
2. Khanadeev V.A., Khlebtsov B.N., Staroverov S.A.,Vidyasheva I.V., Skaptsov A.A., Ileneva E.S., Bogatyrev V.A., Dykman L.A., Khlebtsov N.G. *J. Biophotonics*, **4**, 74 (2011).
3. Beduneau A., Saulnier P., Benoit J.P. *Biomaterials*, **28** (33), 4947 (2007).
4. Cheng Y., Samia A.C., Meyers J.D., Panagopoulos I., Fei B., Burda C. *J. Am. Chem. Soc*., **130**, 10643 (2008).
5. Terentyuk G.S., Maslyakova G.N., Suleymanova L.V., Khlebtsov N.G., Khlebtsov B.N., Akchurin G.G., Maksimova I.L., Tuchin V.V. *J. Biomed. Opt*., **14**, 021016 (2009).
6. Khlebtsov N.G., Dykman L.A. *Chem. Soc. Rev*., **40**, 1647 (2011).
7. Boisselier E., Astruc D. *Chem. Rev.*, **38**, 1759 (2009).
8. Khlebtsov N.G., Dykman L.A. *J. Quant. Spectrosc. Radiat. Transfer*, **111**, 1 (2010).
9. Tuchina E.S., Tuchin V.V., Khlebtsov B.N., Khlebtsov N.G. *Kvantovaya Elektron*., **41** (4), 354 (2011) [*Quantum Electron*., **41** (4), 354 (2011)].
10. Cheng S.-H., Lee C.-H., Chen M.-C., Souris J.S., Tseng F.-G., Yang C.-S., Mou C.-Y., Chen C.-T., Lo L.-W. *J. Mater. Chem*., **20**, 6149 (2010).
11. Bardhan R., Chen W., Bartels M., Perez-Torres C., Botero M.F., McAninch R.W., Contreras A., Schiff R., Pautler R.G., Halas N.J., Joshi A. *Nano Lett*., **10**, 4920 (2010).
12. Paciotti G.F., Myer L., Weinreich D., Goia D., Pavel N., McLaughlin R.E., Tamarkin L. *Drug Delivery*, **11**, 169 (2004).
13. Bisht S., Khan M.A., Bekhit M., Bai H., Cornish T., Mizuma M., Rudek M.A., Zhao M., Maitra A., Ray B., Lahiri D., Maitra A., Anders R.A. *Laboratory Investigation*, **91**, 1383 (2011).
14. Ribeiro C., Neto A.P., das Neves J., Bahia M.F., Sarmento B. *Methods Molec. Biol*., **811**, 113 (2012).
15. Pulavendran S., Rose C., Mandal A.B. *J. Nanobiotechnol*., **9** (15), 1 (2011).
16. Tranberg K.-G., Myllymäki L., Möller P.H., Ivarsson K., Sjögren H.O., Stenram U. J. *X-Ray Sci. Technol.*, **10**, 177 (2002).
17. Germer C.T., Albrecht D., Isbert C., Ritz J., Roggan A., Buhr H.J. *Lasers Med. Sci.*, **14**, 32 (1999).
18. Maksimova I.L., Akchurin G.G., Terentyuk G.S., Khlebtsov B.N., Akchurin G.G., Jr., Ermolayev I.A., Skaptsov A.A., Revzina E.M., Tuchin V.V., Khlebtsov N.G. *Kvantovaya Elektron*., **38** (6), 536 (2008) [*Quantum Elelctron*., **38** (6), 536 (2008)].
19. Kirillin M., Shirmanova M., Sirotkina M., Bugrova M., Khlebtsov B., Zagaynova E. *J. Biomed. Opt*., **14** (2), 021017 (2009).
20. Kim C.S., Wilder-Smith P., Ahn Y.-C., Liaw L.-H., Chen Z., Kwon Y.J. *J. Biomed. Opt*., **14** (3), 034008 (2009).
21. Drexler W., Fujimoto J.G. (Eds) *Optical Coherence Tomography: Technology and Application*s (Berlin, Heidelberg: Springer-Verlag, 2008) p. 1330.
22. Fercher A.F., Drexler W., Hitzenberger C.K., Lasser T. *Rep. Prog. Phys*., **66**, 239 (2003).
23. Dolin L.S., Feldchtein F.I., Gelikonov G.V., Gelikonov V.M., Gladkova N.D., Iksanov R.R., Kamensky V.A., Kuranov R.V., Sergeev A.M., Shakhova N.M., Turchin I.V., in *Coherent-Domain Optical Methods: Biomedical Diagnostics, Environmental and Material Science.* Ed. by V.V.Tuchin (Boston: Kluwer Acad. Publ.) Vol. 2, p. 211.
24. Wang R.K., Tuchin V.V., in *Coherent-Domain Optical Methods: Biomedical Diagnostics, Environmental and Material Science.* Ed. by Tuchin V.V. (Boston: Kluwer Acad. Publ., 2004) Vol. 2, p. 3.
25. Cang H., Sun T., Li Z.-Y., Chen J., Wiley B.J., Xia Y. *Opt.Lett*., **30** (22), 3048 (2005).
26. Genina E.A., Kinder S.A., Bashkatov A.N., Tuchin V.V. *Izv. SGU. Ser. Fiz.*, **11** (2), 10 (2011).
27. Klebtsov B.N., Khanadeev V.A., Maksimova I.L., Terentyuk G.S., Khlebtsov N.G. *Rossiyskie Nanotekhnologii*, **5** (7-8), 54 (2010).
28. Xia Y., Li W., Cobley C.M., Chen J., Xia X., Zhang Q., Yang M., Cho E.Ch., Brown P.K. *Acc. Chem. Res*., **44** (10), 914 (2011).
29. Borzyak E.I., Volkova L.I., Dobrovol'skaya E.A., Revazov V.S., Sapin M.R. *Anatomiya cheloveka. Pod. red. M.R. Sapina* (Human Anatomy. Ed. by M.R. Sapin) (Moscow: Meditsina, 1993) Vol. 1, p. 544.
30. Blouin A., Bolender R.P., Weibel E.R. *J. Cell Biol.*, **72**, 441 (1977).
31. Tuchin V.V. *Lazery i volokonnaya optika v biomeditsinskikh issledovaniyakh* (Lasers and Fibre Optics in Biomedical Studies) (Moscow: Fizmatlit, 2010) p. 488.
32. Gambichler T., Matip R., Moussa G., Altmeyer P., Hoffmann K. *J. Dermatol. Sci*., **44**, 145 (2006).